Selective Detection of Angular-Momentum-Polarized Auger Electrons by Atomic Stereography

Fumihiko Matsui,[1,*] Masayoshi Fujita,[1] Takuya Ohta,[1] Naoyuki Maejima,[1] Hirosuke Matsui,[1] Hiroaki Nishikawa,[1] Tomohiro Matsushita,[2] and Hiroshi Daimon[1]

[1]*Graduate School of Materials Science, Nara Institute of Science and Technology, 8916-5 Takayama, Ikoma, Nara 630-0192, Japan*

[2]*Japan Synchrotron Radiation Research Institute (JASRI), SPring-8, Sayo, Hyogo 679-5198, Japan*

(Received 1 August 2014; revised manuscript received 23 November 2014; published 7 January 2015)

When a core level is excited by circularly polarized light, the angular momentum of light is transferred to the emitted photoelectron, which can be confirmed by the parallax shift of the forward focusing peak (FFP) direction in a stereograph of atomic arrangement. No angular momentum has been believed to be transferred to normal Auger electrons resulting from the decay process filling core hole after photoelectron ejection. We succeeded in detecting a non-negligible circular dichroism contrast in a normal Auger electron diffraction from a nonmagnetic Cu(001) surface far off from the absorption threshold. Moreover, we detected angular-momentum-polarized Cu $L_3M_{4,5}M_{4,5}$ Auger electrons at the L_3 absorption threshold, where the excited core electron is trapped at the conduction band. From the kinetic energy dependence of the Auger electron FFP parallax shift, we found that the angular momentum is transferred to the Auger electron most effectively in the case of the $^1S_0$ two-hole creation.

DOI: 10.1103/PhysRevLett.114.015501 PACS numbers: 61.05.js, 79.20.Fv

Photoelectron spectroscopy and diffraction are powerful techniques to analyze electronic and atomic structures, respectively [1]. Forward focusing peaks (FFPs) appearing in the photoelectron intensity angular distribution (PIAD) indicate the directions of atoms surrounding a photoelectron emitter atom [2]. When a core level is excited by a circularly polarized light (CPL), the angular momentum of light is transferred to the emitted photoelectron, which can be confirmed by taking a stereograph of the atomic arrangement and measuring the parallax shift of the FFP direction [3]. Therefore, by setting a detector at the corresponding position, photoelectrons with a specific angular momentum can be selectively detected. At the same time, an orbital-momentum-polarized hole state is generated. Thus, photoexcitation is an excellent way to extract polarized core electrons as well as valence electrons with a specific orbital momentum in a controlled fashion localized in space and precise in time.

Figure 1(a) shows the wave function of a photoelectron in a (001) plane emitted from a Cu $3d$ level excited with positive helicity ($\sigma = 1$) CPL calculated by using a multiple scattering simulation code: TMSP [4]. The photoelectron is partially scattered by the surrounding atoms. Direct and scattered waves interfere and form a photoelectron diffraction pattern, particularly FFPs at the directions of surrounding scattering atoms. The photoelectron wave propagates toward the direction perpendicular to the photoelectron isophase plane. The isophase plane of the photoelectron direct wave is spiral in the case of CPL excitation. Note that the direction of FFP rotates around the incident light axis toward the same direction as the helicity of CPL. The rotation angle $\Delta\phi$ is well described by the Daimon formula

$$\Delta\phi = \tan^{-1}\frac{m_f^*(\theta_{\rm out})}{kR\sin^2\theta_{\rm out}}, \quad (1)$$

where $m_f^*(\theta_{\rm out})$ and k are the angular momentum and the wave number of the photoelectron, respectively [3,5]. $\theta_{\rm out}$ is the angle between the incident photon axis and the outgoing direction of the emitted photoelectrons. The shift is inversely proportional to the interatomic distance R between the photoelectron emitter and the scatterer atoms. Thus, the local stereoscopic atomic arrangements can be imaged directly with a stereograph which consists of a pair of PIADs excited by CPL [3,5–7].

The effective magnetic quantum number $m_f^*(\theta_{\rm out})$ is the average of the different final state angular momenta m_f from the initial states of quantum number $m_i = m_f - \sigma$ weighted by the transition probability at $\theta_{\rm out}$ [8]. $m_f^*(\theta_{\rm out})$ for a $l_i \to l_f = l_i + 1$ channel is as follows.

$$m_f^*(\theta_{\rm out}) = \frac{\sum_{m_i=-l_i}^{l_i} m_f |c^1(l_f, m_f, l_i, m_i)\Theta_{l_f,m_f}|^2}{\sum_{m_i=-l_i}^{l_i} |c^1(l_f, m_f, l_i, m_i)\Theta_{l_f,m_f}|^2}, \quad (2)$$

where c^1 is the Gaunt coefficient. Θ_{l_f,m_f} is a spherical harmonics which determines the polar angle dependence of the transition matrix element. As shown in Fig. 1(b), contributions to $m_f^*(90°)$ for $m_f = 0$ and 2 will be 0, while that of m_f with ± 1 will be 0 at $\theta_{\rm out} = 63.43°$. By setting the appropriate incident angle, the photoelectron with specific angular momentum m_f can be excluded.

The prominent FFP circular dichroism was also observed in the valence band PIADs at the high kinetic energy of around 500 eV [9]. The rotational shift of the photoelectron

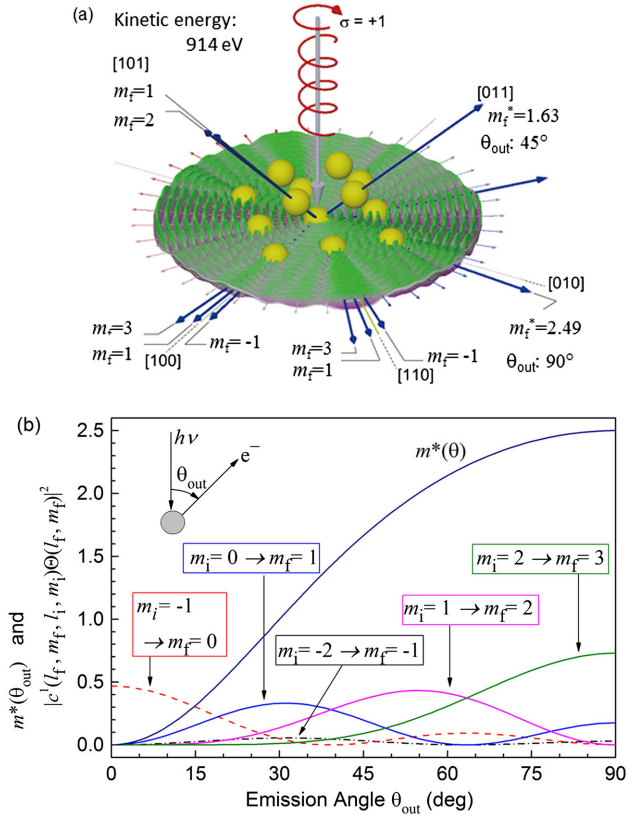

FIG. 1 (color online). (a) Real part of a simulated Cu 3*d* photoelectron wave function from a 13-atom Cu fcc cluster excited by a circularly polarized soft x ray. (b) Polar angle dependence of angular momentum of the photoelectron from the 3*d* state.

FFP derived for the σ_{xy} band was twice those for π and 2*s* bands, indicating that the FFP shift can be used to measure the orbital angular momentum of atomic orbitals constituting each of the energy bands. However, no angular momentum was believed to be transferred to the Auger electrons resulting from the decay process filling the core hole after photoelectron emission. But when the excited core electron is trapped at the conduction band, an extraordinarily large angular momentum transfer to the resonant Auger electron was found by Morscher *et al.* [10] for Ni L_2 absorption. Here we report a quantitative analysis of angular-momentum-polarized $L_3M_{4,5}M_{4,5}$ Auger electrons from a nonmagnetic Cu(001) surface at the L_3 absorption threshold. Based on the angular momentum analysis of the Auger electron, we clarified the mechanism of circular dichroism in Auger electron diffraction.

The single-crystalline Cu(001) surface was sputtered with Ar^+ ions and annealed up to 500 °C in ultra-high-vacuum condition to obtain a clean surface. The quality of the substrate surface was checked by reflection high energy electron diffraction, Cu photoelectron spectroscopy, and their angular distributions [11,12]. Cu 3*d* PIAD and *LMM* Auger electron intensity angular distributions (AIADs) were measured using a display-type spherical mirror analyzer (DIANA) [13,14] at the circularly polarlized soft x-ray beam line BL25SU of SPring-8, Japan [15]. The helicity ($\sigma = \pm 1$) of monochromatized CPL was reversed by switching the path of storage ring electrons in twin helical undulators at 0.1 Hz [16]. The acceptance angle of the analyzer was ±60°. Electrons emitted from the sample were energy analyzed, and their angular distributions were projected onto the fluorescent screen. The photon energy resolution was about 100 meV. For the full hemisphere angular distribution measurement, the energy window width of DIANA was set to 5% of 914 eV and the whole intensity of the valence band or $L_3M_{4,5}M_{4,5}$ Auger electrons were integrated, while the energy window width was set to 2 eV for measuring kinetic energy dependence of the FFP shift for LMM Auger electrons.

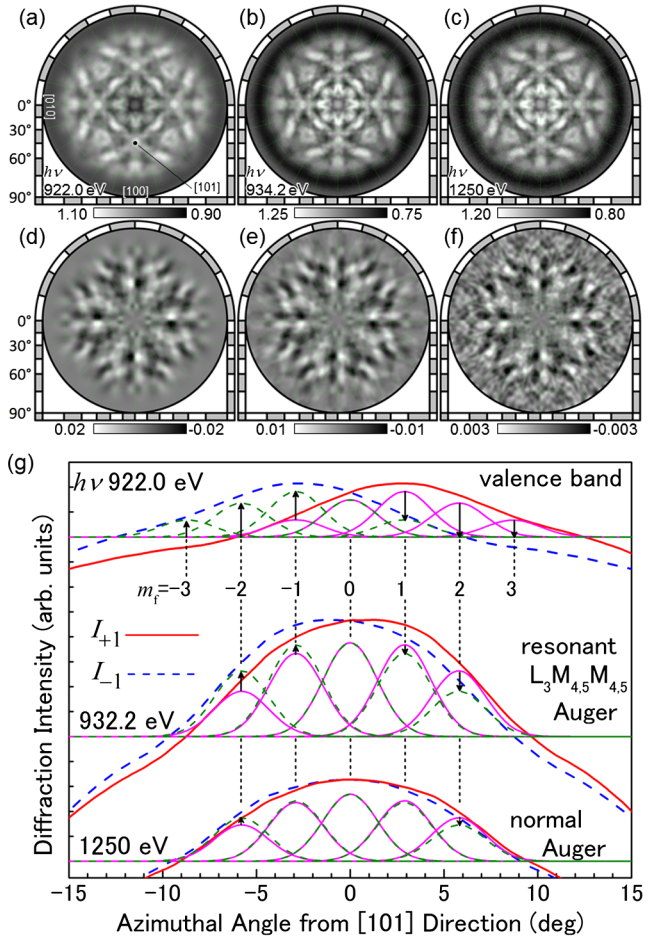

FIG. 2 (color online). Full hemisphere angular distribution of (a) Cu valence band photoelectron at the kinetic energy of 914 eV excited by a circularly polarized soft x ray at a photon energy of 922 eV. (b) and (c) Same as (a) but for $L_3M_{4,5}M_{4,5}$ Auger electrons at the photon energy of 934.2 and 1250 eV, respectively. (d)–(f) Circular dichroism angular distributions of (a)–(c), respectively. (g) Azimuthal profiles of [101] FFP intensity for photoelectron and Auger electrons.

Figure 2(a) shows a full hemisphere PIAD of a valence band, mainly from Cu $3d$ orbitals, at the kinetic energy of 914 eV excited by 922 eV CPL. Details of PIAD data processing are described elsewhere [17]. PIADs excited by both helicities ($\sigma = \pm 1$) were added. Note that at this kinetic energy, FFP is also present even for a delocalized valence band due to the majority of excitation coming from electron density existing at the vicinity of nucleus [9]. The FFP at the four $\langle 101 \rangle$ directions corresponds to the scattering by the nearest neighbor atoms, while the center [001] direction corresponds to the second nearest neighbor atoms along the surface normal. The FFP is about 10° in diameter. Figures 2(b) and 2(c) show resonant and normal Cu $L_3M_{4,5}M_{4,5}$ AIADs at the kinetic energy of 914 eV excited by CPL with a photon energy of 934.2 and 1250 eV, respectively. The diffraction pattern is formed by the interference of the direct excitation wave Ψ_0 and scattered waves Ψ_i by surrounding atoms. All three angular distributions were basically similar. The reason for the similarity between PIAD and AIADs is owing to the scattered waves Ψ_i mainly determined by the same atomic arrangement and the same wave number of the electron. The excitation mechanism difference makes the difference in Ψ_0. In detail, the diffraction pattern contrasts around the [001] direction were higher in the Auger electron cases than that of the photoelectron, since Ψ_0 is more isotropic in the cases of the Auger electron [11,18].

Figure 2(d) shows the difference of the two PIADs excited by both helicities and normalized by the sum: $(I_1 - I_{-1})/(I_1 + I_{-1})$. The suffix denotes the helicity. Figures 2(e) and 2(f) show the circular dichroism of resonant and normal AIADs, respectively. This result indicates that at the L_3 absorption threshold, where the excited core electron is trapped at the conduction band, the angular momentum was partially transferred to resonant $L_3M_{4,5}M_{4,5}$ Auger electrons instead. Furthermore, even a non-negligible circular dichroism contrast ($\pm 3 \times 10^{-3}$) in a normal Auger electron diffraction far off from the absorption threshold was detected. This is a surprising result, since no angular momentum was believed to be transferred to the normal Auger electrons. Note that the kinetic energy of $3p$ and $3s$ photoelectrons is 1170 and 1130 eV, respectively, which is over 200 eV larger than the kinetic energy of the Auger electron. Circular dichroism of those energy-loss photoelectrons at the kinetic energy of 914 eV is estimated to be no more than 1×10^{-4} and negligible [19].

Each azimuthal profile of the [101] FFP intensity was fitted with Gaussians centered at $\phi = m_f \times 2.894°$ directions corresponding to the different angular momenta of emitted electrons as shown in Fig. 2(g). Note that the photoelectrons from the $3d$ valence band gain angular momentum σ by CPL excitation, while the angular momenta of LMM Auger electrons are the same as $3d$ valence electrons. The components of $m_f = \pm 3$ do not exist in the FFP of AIAD as shown in Fig. 2(g). The origin of circular dichroism in the resonant AIAD is attributed to the difference in transition to the final states $m_f = \pm 1$ as well as ± 2.

The transition to the final states $m_f = \pm 2$ is forbidden at $\theta_{\text{out}} = 90°$ geometry as seen in Fig. 1(b). By setting the incident light axis along the $[\bar{1}01]$ direction, the emission angle for [101] FFP became 90°. By using FFP shifts with different incident angle conditions, the angular momentum m_f selective Auger electron can be detected.

Figure 3(a) shows the kinetic energy dependences of the [101] FFP circular dichroism contrast for 45° and 90° emission geometries. Figure 3(b) shows the kinetic energies and relative intensities of $L_3M_{4,5}M_{4,5}$ Auger electrons having different final states [20,21]. The Auger electron intensity was largest at 914 eV corresponding to the $^1G_4$ two-hole state, while the circular dichroism contrast was largest at 910 eV corresponding to the satellite peak of the $^1S_0$ two-hole state. From the comparison of two energy dependence, the transition to $m_f = 1$ and 2 were found to be dominant at 910 and 914 eV, respectively.

Figure 4(a) shows the $2p$ photoelectron emission process, while 4(b) and 4(c) summarize the resonant Auger emission process. At the L_3 absorption threshold, the $2p$ core electron is excited to the $4s$ conduction band. Since the $4s$ state has an angular momentum of 0, the orbital-momentum-polarized core hole with $m = \mp 1$ is created by $\sigma = \pm 1$ excitation as shown in Fig. 4(b). Several Auger decay paths with different final states exist. The final state can be selected by the energy analysis of the Auger

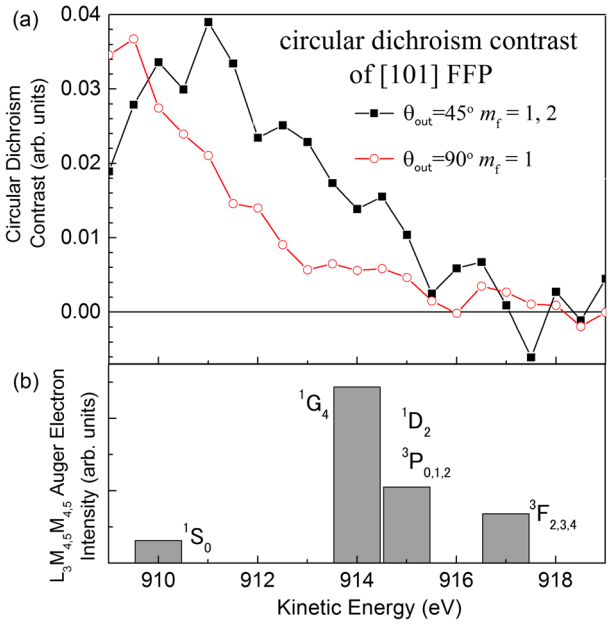

FIG. 3 (color online). (a) Circular dichroism contrast of a forward focusing peak at the [101] direction for an emission angle of 45° and 90°. (b) Kinetic energy and intensity of Auger electron [20,21]. The term symbol for each multiplet peak is indicated.

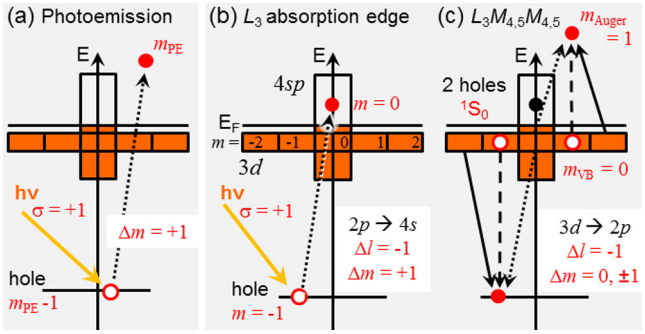

FIG. 4 (color online). Schematic diagrams of (a) the photoemission process and (b) x-ray absorption at the L_3 edge together with (c) succeeding $L_3M_{4,5}M_{4,5}$ Auger electron emission.

electron. Figure 4(c) is the schematic diagram of the succeeding $L_3M_{4,5}M_{4,5}$ process for the $^1S_0$ two-hole final state. The final state $^1S_0$ consists of two hole states having angular momentum with an opposite sign ($m_i = \pm 2$, $m_i = \pm 1$, or two electrons with $m_i = 0$). When a valence electron with $m_i = -1$ decays to fill the $2p$ core hole, another valence counterpart with $m_i = 1$ is emitted as the $L_3M_{4,5}M_{4,5}$ Auger electron of $^1S_0$. When valence electrons with $m_i = -2$ and 0 decay, the counterparts will be the ones with $m_i = 2$ and 0, respectively. Since the angular momentum is conserved throughout the whole process, the Auger electron with $m_f = 1$ is emitted.

The two-hole states of the final state $^1S_0$ at the bottom of the $3d$ band correspond to t_{2g} atomic orbitals, i.e., $3d_{zx}$, $3d_{yz}$, and $3d_{xy}$. These orbitals form σ bonds between neighboring Cu atoms. These orbitals are selectively detected in the circular dichroism contrast in the $^1S_0$ Auger excitation process.

In conclusion, we have measured full hemisphere intensity angular distributions of the $L_3M_{4,5}M_{4,5}$ Auger electron excited by CPL with a photon energy of 934.2 and 1250 eV, as well as that of the $3d$ photoelectron. We detected a non-negligible circular dichroism contrast in a normal Auger electron diffraction far off from the absorption threshold. This suggests that the Cu $2p$ core hole state generated after photoelectron excitation to the continuum state is slightly angular-momentum polarized. In the case of the resonant Auger electron where the excited core electron is trapped at the conduction band, the circular dichroism was much enhanced. Moreover, from the kinetic energy dependence of the Auger electron FFP parallax shift, we found that the angular momentum is transferred to the Auger electron most effectively in the case of the $^1S_0$ two-hole creation. This method has a great advantage in doping the hole state in the valence band as compared to the simple valence band photoexcitation, especially in the case of the compound crystal owing to the element selectivity and high sensitivity of Auger electron emission.

This work was performed with the approval of the Japan Synchrotron Radiation Research Institute (Proposals No. 2013A1440 and No. 2013B1307). The authors deeply thank Dr. Takayuki Muro, Dr. Tetsuya Nakamura, and Dr. Toyohiko Kinoshita for their support in the experiments. This research was supported by JSPS Grant-in-Aid for Young Scientists (B) 22740200, 2010, for Scientific Research (B), 25287075, 2013, and for Scientific Research on Innovative Areas "3D Active-Site Science": 26105007 2604.

*Corresponding author.
matui@ms.naist.jp

[1] C. S. Fadley, J. Electron Spectrosc. Relat. Phenom. **178–179**, 2 (2010).
[2] W. F. Egelhoff, Jr., Phys. Rev. B **30**, 1052 (1984).
[3] H. Daimon, Phys. Rev. Lett. **86**, 2034 (2001).
[4] http://sourceforge.jp/projects/tmcoca/.
[5] H. Daimon, T. Nakatani, S. Imada, S. Suga, Y. Kagoshima, and T. Miyahara, Jpn. J. Appl. Phys. **32**, L1480 (1993).
[6] F. Matsui, T. Matsushita, and H. Daimon, J. Electron Spectrosc. Relat. Phenom. **178–179**, 221 (2010).
[7] F. Matsui, N. Nishikayama, N. Maejima, H. Matsui, K. Goto, M. Hashimoto, T. Hatayama, T. Matsushita, Y. Kato, and H. Daimon, J. Phys. Soc. Jpn. **80**, 013601 (2011).
[8] H. Daimon, S. Imada, and S. Suga, Surf. Sci. **471**, 143 (2001).
[9] F. Matsui, T. Matsushita, Y. Kato, F. Z. Guo, and H. Daimon, J. Phys. Soc. Jpn. **76**, 013705 (2007).
[10] M. Morscher, F. Nolting, T. Brugger, and T. Greber, Phys. Rev. B **84**, 140406(R) (2011).
[11] T. Matsushita, F. Z. Guo, F. Matsui, Y. Kato, and H. Daimon, Phys. Rev. B **75**, 085419 (2007).
[12] F. Matsui, T. Matsushita, Y. Kato, M. Hashimoto, K. Inaji, F. Z. Guo, and H. Daimon, Phys. Rev. Lett. **100**, 207201 (2008).
[13] H. Daimon, Rev. Sci. Instrum. **59**, 545 (1988).
[14] M. Kotsugi, Y. Miyatake, K. Enomoto, K. Fukumoto, A. Kobayashi, T. Nakatani, Y. Saitoh, T. Matsushita, S. Imada, T. Furuhata, S. Suga, K. Soda, M. Jinno, T. Hirano, K. Hattori, and H. Daimon, Nucl. Instrum. Methods **467–468**, 1493 (2001).
[15] Y. Saitoh, H. Kimura, Y. Suzuki, T. Nakatani, T. Matsushita, T. Muro, T. Miyahara, M. Fujisawa, K. Soda, S. Ueda, H. Harada, M. Kotsugi, A. Sekiyama, and S. Suga, Rev. Sci. Instrum. **71**, 3254 (2000).
[16] T. Muro, T. Nakamura, T. Matsushita, H. Kimura, T. Nakatani, T. Hirono, T. Kudo, K. Kobayashi, Y. Saitoh, M. Takeuchi, T. Hara, K. Shirasawa, and H. Kitamura, J. Electron Spectrosc. Relat. Phenom. **144–147**, 1101 (2005).
[17] F. Matsui, T. Matsushita, and H. Daimon, J. Electron Spectrosc. Relat. Phenom. **195**, 347 (2014).
[18] H. Li and B. P. Tonner, Phys. Rev. B **37**, 3959 (1988).
[19] F. Matsui, M. Hashimoto, T. Matsushita, K. Goto, N. Maejima, H. Matsui, Y. Kato, and H. Daimon, J. Phys. Soc. Jpn. **81**, 013601 (2012).
[20] I. Coulthard, T. K. Sham, Y.-F. Hu, S. J. Naftel, P.-S. Kim, and J. W. Freeland, Phys. Rev. B, **64**, 115101 (2001).
[21] A. Föhlisch, O. Karis, M. Weinelt, J. Hasselström, A. Nilsson, and N. Mårtensson, Phys. Rev. Lett., **88**, 027601 (2001).